THE JOURNAL OF PHYSICAL CHEMISTRY LETTERS
A JOURNAL OF THE AMERICAN CHEMICAL SOCIETY

pubs.acs.org/JPCL

Letter

Conformer-Specific Tunneling Dynamics Dictated by the Seam Coordinate of the Conical Intersection

Kyung Chul Woo, Junggil Kim, and Sang Kyu Kim*

Cite This: *J. Phys. Chem. Lett.* 2021, 12, 1854−1861

Read Online

ACCESS | Metrics & More | Article Recommendations | Supporting Information

ABSTRACT: The dynamic role of the conical intersection "seam" coordinate has been first revealed in the H fragmentation reaction of *ortho(o)*-cresol conformers. One of the $(3N-8)$ dimensional seam coordinates of the $S_1(\pi\pi^*)/S_2(\pi\sigma^*)$ conical intersection has been identified as the CH_3 torsional potential function. The tunneling dynamics of the reactive flux is dictated by its nuclear layout with respect to the CH_3 torsional angle, as the multidimensional tunneling barrier is dynamically shaped along the conical intersection seam. The effective tunneling-barrier weight-averaged over the quantum-mechanical probability along the CH_3 torsional angle perfectly explains the experimental finding: the sharp variation of the tunneling rate ($(700-400)$ ps^{-1}) with the CH_3 torsional mode excitations within the narrow ($0-100$ cm^{-1}) energetic window. The much longer S_1 lifetime of *cis* compared to *trans* is ascribed to the higher-lying S_1/S_2 conical intersection of the former. With the use of distinct lifetimes, vibronic bands of each conformer could be completely separated.

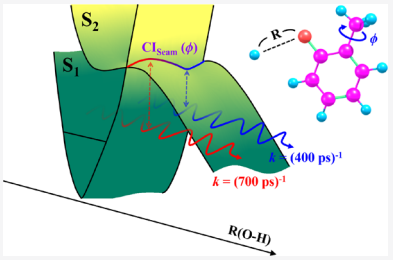

In order to understand the multidimensional aspects of chemical reactions, the relationship between the molecular structure and the chemical reactivity should be firmly established, as chemical reactions do not start from a frozen single-molecular structure. Internal rotations about the single bonds in the polyatomic molecules give rise to a number of conformational isomers, and these structural isomers are expected to take their own characteristic reaction pathways, which are nontrivial to invoke individually in ambient conditions. Even when the structural differences of conformers are subtle, the chemical reactivity could be largely influenced. Nature wisely utilizes the conformational changes as a tool for the control of chemical or biological processes. Because of the facile interconversion of conformational isomers, however, it is nontrivial to interrogate the conformer-specific chemistry in the condensed phases. In this sense, the vibrational/rotational cooling in the molecular jet provides a great opportunity to investigate the conformational specificity of the chemical reaction. When several conformational isomers are prepared in their local minima, it is in principle plausible to select just one conformational isomer at a time by using the spectroscopic and/or Stark deflection method. Further exploration of the dynamics of photodissociation, ionization, or bimolecular collisional processes then gives the unique chance for unraveling the conformer-specific chemical reactivity in molecular detail. In reality, however, investigations of the conformer-selective dynamics have been quite rare, except a few outstanding examples. These include the photodissociation dynamics of the 1-iodopropane cation[1] or the 1-propanal cation.[2,3] In these experiments, a specific conformational isomer of the cation was exclusively chosen spectroscopically, leading to the experimental observation of the distinct conformer-specific photodissociation dynamics. A recent report regarding the bimolecular reaction of Ca^+ in the Coulomb crystal with the spatially separated[4] *cis* or *trans* conformer of 3-aminophenol is also quite notable, as it shows the dramatic conformer specificity in the ion-neutral bimolecular reaction.[5,6] The structural effect on the chemical reactivity of neutral molecules could be found in the conformer-specific excited-state lifetimes as demonstrated in a nonradiative deactivation of model peptides[7] or micro-hydrated nucleic acids,[8] among many other examples.

Photodissociation of the S_1 phenol has been intensively investigated for recent decades not only because it represents photochemistry of the basic biological building block but also because it is the prototypical system of the $\pi\sigma^*$-mediated relaxation process, which has gotten much interest in recent years.[9−29] It has been well-established that the phenol in S_1 loses the hydrogen atom from its OH moiety via tunneling through the adiabatic reaction barrier under the S_1/S_2 conical intersection where $S_1(\pi\pi^*)$ is bound, whereas S_2 $(\pi\sigma^*)$ is repulsive with respect to the O−H bond elongation coordinate. Nonradiative transitions other than the H atom tunneling occur concomitantly with a rate of $\sim(12\text{ ns})^{-1}$.[30−35] As the H atom detachment via tunneling is relatively much faster, the measured lifetime (τ) of ∼2.3 ns at the S_1 zero-point

Received: December 21, 2020
Accepted: February 8, 2021

https://dx.doi.org/10.1021/acs.jpclett.0c03742
J. Phys. Chem. Lett. 2021, 12, 1854−1861

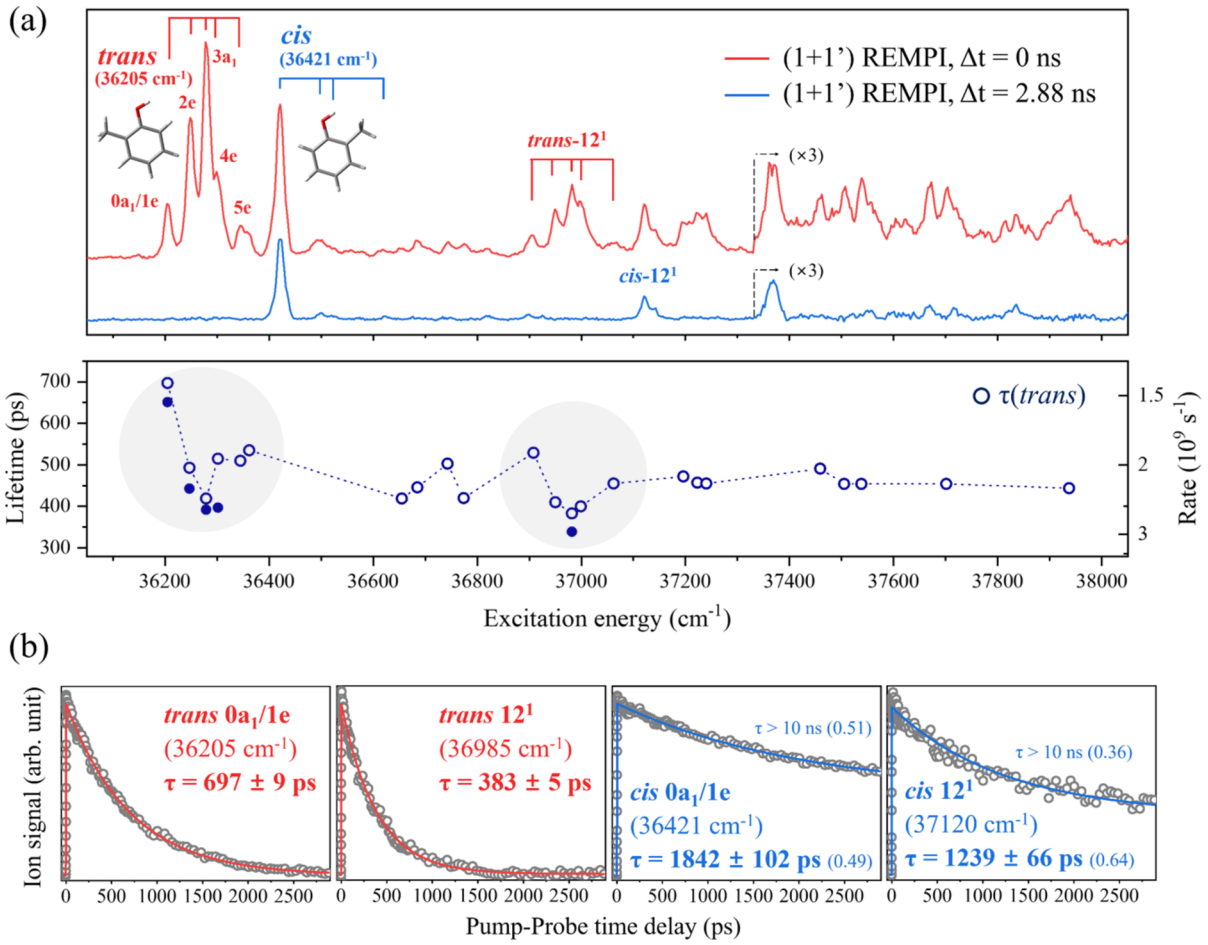

Figure 1. Conformer-specific S_1-S_0 vibronic transitions and S_1 lifetimes. (a) Picosecond (1 + 1′) R2PI spectrum of *o*-cresol taken at the zero delay time (black solid) and the delay time of 2.88 ns (blue solid). The CH_3 torsional progression bands are denoted by the combs for the *trans* (red) or *cis* (blue) conformer. The signal due to the *trans* conformer is more strongly observed compared to that of the *cis* conformer in the R2PI spectrum taken at the zero time delay, implying that the trans conformer is relatively more populated in the current experimental jet condition. The state-specific S_1 lifetimes obtained from the parent ion transients (open) or the H^+ growth curves (closed) for the *trans* conformer are shown in the lower part. (b) The parent transients of the *trans*-*o*-cresol (red) or *cis*-*o*-cresol (blue) taken at the zero-point vibrational level ($0a_1/1e$) or excited vibrational level (12^1 mode) of each. For the *cis*-*o*-cresol, the relative weighting factors used in the biexponential fits are denoted in parentheses. For the full transients and fits, see the Supporting Information.

level mainly reflects the tunneling rate of phenol.[24,30−32,36−39] From our recent picosecond time-resolved transients for both parent and fragment, it has been found that the tunneling rate largely fluctuates with some low-frequency vibrational mode excitations until it converges above the S_1 internal energy of ~1500 cm^{-1}.[39] This experimental finding already indicates that the tunneling process of the S_1 phenol is multidimensional in nature, and tunneling barriers are dynamically shaped with respect to a variety of nuclear configurations characterized by the specific vibronic excitations.

To further explore the outstanding question of the conformer specificity in the tunneling process, we investigate here the reaction rates of the S_1 state of a *cis*- or *trans*-conformer of *o*-cresol in the molecular jet. Especially, the structural effect induced by the CH_3 internal rotation on the overall S_1 dephasing dynamics is our focus here. The S_1-S_0 vibronic transitions of *o*-cresol had been spectroscopically intensively studied by many groups.[40−45] According to them, compared to the threefold CH_3 torsional barrier (V_3) of 355 (600) cm^{-1} in the ground S_0 state of *trans*- (*cis*-) *o*-cresol, it becomes quite shallow in the first excited S_1 state to give V_3 = 83 (90) cm^{-1}.[42−44] It was also found that the *cis* conformer adopts the CH_3 staggered geometry in both S_0 and S_1, whereas the staggered geometry in S_0 undergoes the structural change to the eclipsed geometry upon the S_1-S_0 transition for the *trans* conformer (vide infra). Also note that the photofragmentation dynamics of each conformer had been thoroughly studied by the high-resolution H atom translational spectroscopic method,[45] whereas the S_1 excited lifetimes of the origin transitions of *trans* and *cis* had been reported to be 0.70 and 3.0 ns, respectively.[31] Herein, we report the conformer-specific H atom tunneling dynamics of two conformational isomers of *o*-cresol in the first electronically excited state. Especially, we found that the internal rotation of the methyl moiety of the *o*-cresol exerts a strong influence on the H atom tunneling dynamics, although it is remote and seems to be irrelevant.

Intuitively, it is anticipated that the H atom tunneling dynamics of *o*-cresol is little different from that of phenol, as the methyl substitution on the phenyl moiety would least modify characteristics of electronic states in general. And yet, *trans* and *cis* conformers of *o*-cresol, which could be interconverted by the internal rotation about the single C−O(H) bond, are found to be dramatically different in their

https://dx.doi.org/10.1021/acs.jpclett.0c03742
J. Phys. Chem. Lett. 2021, 12, 1854−1861

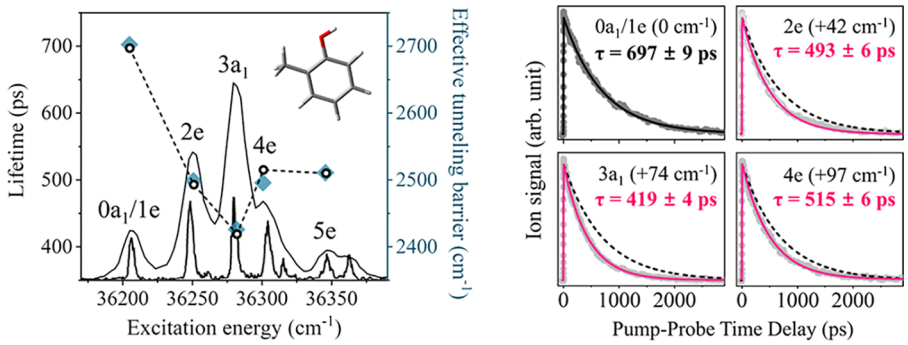

Figure 2. Tunneling dynamics controlled by the CH_3torsional mode excitation. (left) The S_1 lifetimes (open circles belonging to the left ordinate) measured from the parent ion transients of the *trans-o*-cresol with the CH_3 torsional mode excitations. The effective tunneling barrier (filled diamonds belonging to the right ordinate) calculated from the weight average over the CH_3 torsional angle based on the individual torsional mode wave function (see the text). The picosecond (1 + 1′) R2PI spectrum is overlaid with the previously reported nanosecond R2PI spectrum (reprinted from ref 44). (right) The parent transients of the *trans-o*-cresol for the first few CH_3 torsional mode excitations. The transient at the zero-point level ($0a_1/1e$) is denoted as the black dotted line for comparison with other transients.

tunneling rates. Different S_1 lifetimes of *cis* and *trans* conformers as well as their mode dependencies are interrogated thoroughly in this work by using the state-selective and time-resolved picosecond pump−probe technique. The S_1 and S_2 potential energy surfaces along the O−H elongation coordinate for all possible conformational isomers of *o*-cresol are obtained from high-level ab initio calculations. The huge difference in lifetimes of the *cis* and *trans* conformers makes it possible to completely differentiate the S_1 vibronic bands of specific conformers in the two-color two-photon resonant ionization spectroscopy employing the different delay times between excitation (pump) and ionization (probe) laser pulses, giving the unambiguous conformational identification for all observed S_1 quantum levels of the title molecule.

Resonance-enhanced two-photon ionization (R2PI) spectra taken using the (1 + 1′) two-color scheme with the picosecond laser pulse are shown in Figure 1. As the delay time (Δt) between the pump (S_1−S_0) (278−261 nm) and probe (D_0−S_1) (281 nm) laser pulses is changed, the R2PI spectrum becomes dramatically different. Namely, a significant number of vibronic bands observed in the R2PI spectrum taken near the time-zero almost completely disappear in that obtained at the delay time of ∼2.9 ns, while the other vibronic bands retain their reduced but significant intensities. This is due to the different S_1 lifetimes of *cis* and *trans* conformers of *o*-cresol (vide infra). A parent ion transient of the *trans-o*-cresol at its S_1 origin, taken with the pump−probe cross-correlation temporal width of 1.2 ps, shows the rapid decay of the S_1 state with the lifetime of 697 ± 9 ps (Figure 1).[31] The transient is nicely fit using a single-exponential decay function implying the complete disappearance of the ion signal at the asymptotic limit. On the other hand, the parent ion transient of the *cis* conformer seemingly shows the biexponential behavior representing the initial decay of the signal with a time constant of ∼1.8 ns along with the long-surviving signal persisting even at the much longer delay time, although the analysis needs to be invoked in more detail (Supporting Information). The distinct difference in lifetimes of *cis* and *trans* conformers of *o*-cresol makes it possible to identify conformer-specific vibronic bands almost perfectly. This provides a new way of differentiating the conformers in the molecular beam, and it may be called a "chrono"-spectroscopy, as it uses the distinct conformer-specific lifetimes of different conformer species. Similarly to the case of phenol, the S_1 lifetime measured for both *trans* and *cis* conformers of *o*-cresol is mainly attributed the H atom tunneling reaction. The appearance rates of the nascent H fragment, which are estimated from the series of picosecond time-resolved velocity-map H^+ images with 243.1 nm (2 + 1)-ionization,[39,46] are found to be identical to the S_1 lifetimes regardless of the translational energy, confirming that all the H fragments should result from the H atom tunneling from the parent molecule.

The *trans-o*-cresol undergoes a structural change upon the S_1−S_0 excitation with respect to the methyl internal rotor, giving a number of highly excited CH_3 internal rotor states as manifested in the R2PI spectrum (Figure 1). The CH_3 internal rotor states of *trans-o*-cresol in the jet had been thoroughly studied by Ito and colleagues,[42] giving the threefold barrier height (V_3) of 83 cm^{-1}. As all the Franck−Condon active internal rotor states are quite distinct in the picosecond R2PI spectrum, the state-specific tunneling lifetimes could be unambiguously measured. Quite interestingly, the tunneling rate corresponding to $\tau \approx 697$ ps at the zero-point ($0a_1/1e$) state becomes accelerated with the CH_3 rotor-level excitation, giving $\tau \approx 493$ and ∼419 ps for the 2e or $3a_1$ state, respectively. And then it falls back to ∼515 or ∼510 ps at the higher rotor levels of 4e and 5e, respectively, Figure 2. Considering the small energy increment of the excited CH_3 rotor mode, which should be orthogonal to the O−H elongation coordinate, the sharp variation of the tunneling rate as such is quite unusual. The acceleration and deceleration of the tunneling rate by the CH_3 internal rotor excitation are also similarly observed at the CH_3 torsional progression bands when they are combined with the 12^1 mode at ∼700 cm^{-1} (Figure 1). The tunneling rates measured for other vibronic bands are otherwise more or less maintained at $k \approx (500\ \text{ps})^{-1}$ in the wide internal energy range of 0−2000 cm^{-1}, suggesting that the internal energy given to the S_1 *trans-o*-cresol within the Franck−Condon window, except the CH_3 torsional mode excitation, is hardly utilized to overcome and/or alter the tunneling barrier. This suggests that the seam coordinates other than the CH_3 torsional angle, at least within the Franck−Condon allowed region, do not play the major dynamic role in the tunneling dynamics (vide infra).

From the geometrical aspect alone, it is not straightforward to imagine that the CH_3 torsional motion is strongly associated with the dynamics of the H atom detachment from the OH moiety. This is especially because the S_1/S_2 conical intersection along the O−H elongation, which dictates the

https://dx.doi.org/10.1021/acs.jpclett.0c03742
J. Phys. Chem. Lett. 2021, 12, 1854−1861

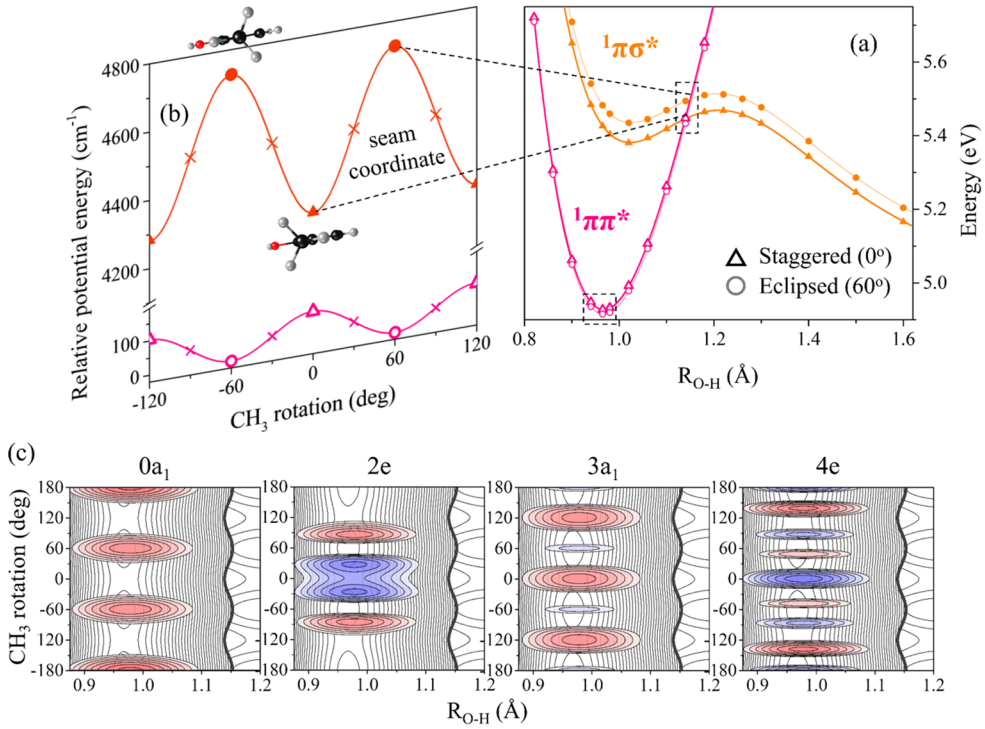

Figure 3. The S_1/S_2 potential energy surfaces of *trans-o*-cresol extended along the conical intersection seam coordinate. (a) Calculated potential energy curves of $\pi\pi^*$ (magenta) and $\pi\sigma^*$ (yellow) states with respect to the O−H bond extension coordinate at the staggered (triangles) or eclipsed (circles) geometry of the CH_3 moiety with respect to the molecular plane. The analytic fits using the Morse-type and exponential functions are shown as solid lines. The vertical excitation energies were estimated with the EOM-CCSD method using the aug-cc-pVDZ basis set from the optimized geometry obtained by the DFT calculation (see the Supporting Information). (b) The sinusoidal torsional potential energy curves at the S_1/S_2 conical intersection (orange) or that at the S_1 minimum energy point (pink) along the CH_3 internal rotation angle. (c) The two-dimensional contour maps of eigenfunctions of the individual CH_3 torsional mode quantum levels on the S_1 potential energy surface. Each contour line of the S_1 potential energy surface has an elevation of 150 cm^{-1}. The conical intersection seam is represented as bold lines.

tunneling reaction through the underlying barrier, is generated on the two-dimensional branching plane of which the gradient vector should be parallel to the O−H elongation coordinate, whereas the most influential coupling vector is along the out-of-plane torsional angle of the OH moiety with respect to the molecular plane.[13] In this sense, the internal rotation of CH_3 with respect to the molecular plane seems to be peripheral from the perspective of the H atom detachment event. To understand this counterintuitive dynamic behavior, the adiabatic potential energy surfaces with respect to the CH_3 internal rotation angle were calculated. In the ground electronic state (S_0) of the *trans-o*-cresol, the CH_3 moiety with respect to the molecular plane adopts the staggered geometry. As the CH_3 torsional barrier height in S_0 is ∼355 cm^{-1} (vide supra),[42] only the nearly degenerate $0a_1/1e$ states of the zero-point level are populated in the molecular jet condition ($T \approx 1$ K). With the S_1-S_0 transition, the *trans-o*-cresol undergoes a structural change from the staggered to eclipsed geometry, as manifested by a number of CH_3 torsional modes excited in the R2PI spectrum (Figure 1). The previously reported spectral analysis for the CH_3 torsional modes in S_1 gives the threefold torsional barrier height of 83 cm^{-1} (vide supra).[42,47] Accordingly, at the S_1 zero-point ($0a_1/1e$) level, the CH_3 torsional geometry should be confined in the eclipsed form. With the CH_3 rotor level excitation, however, the torsional angle spanned by the corresponding eigenstate is largely modulated.

The significant variation of the tunneling rate with the CH_3 torsional mode excitation could be invoked by the equation of motion coupled cluster singles and doubles (EOM-CCSD) calculations of S_1 and S_2 surfaces along the O−H bond extension coordinate for all possible conformational structures based on the vertical energy calculations from the density functional theory (DFT)-optimized S_0 geometry, Figure 3a (see Supporting Information for details). The planar C_s symmetry was maintained during all optimizations. The EOM-CCSD calculation describes the methyl rotor geometry in S_1 extremely well. Consistent with the previous and present spectroscopic evidence, the *cis* conformer remains in the staggered geometry, while the *trans* conformer undergoes the structural change from the staggered to the eclipsed geometry upon the S_1-S_0 transition. The CH_3 torsional barrier in the S_1 state is calculated to be ∼0.01 eV for both conformers, which is in excellent agreement with the previously reported experimental values.[42] Quite intriguingly, the situation is reversed in the S_2 ($^1\pi\sigma^*$) state; the CH_3 staggered geometry is calculated to be more stable than the eclipsed geometry for the *trans* conformer. The torsional potential at the conical intersection is then the sinusoidal function with the eclipsed and staggered conformations as crest and trough, respectively. The CH_3 torsional barrier height at the conical intersection is calculated to be ∼400 cm^{-1}. Notably, the calculated adiabatic S_1 and S_2 potential energy surfaces cross when they are plotted along the OH extension coordinate for both staggered and eclipsed configurations. This suggests that the upper and lower adiabatic states are nearly degenerate at the conical intersection for both geometries, indicating that the S_1/S_2 conical intersection is indeed extended into the seam

https://dx.doi.org/10.1021/acs.jpclett.0c03742
J. Phys. Chem. Lett. 2021, 12, 1854−1861

coordinate of the CH_3 torsional angle with the barrier height of ~400 cm^{-1}. In other words, the CH_3 internal rotation may play an essential dynamic role as one of the $(3N - 8)$ dimensional seam coordinates of the S_1/S_2 conical intersection. The tunneling dynamics would be then quite different for different nuclear layouts in terms of the CH_3 torsional angle. We calculated the eigenfunctions of the CH_3 torsional quantum levels in S_1 by diagonalizing a Hamiltonian matrix using the free-rotor basis set (Supporting Information), Figure 3c. As expected, the wave function is confined in the eclipsed geometry at the zero-point level, whereas it becomes dispersed over the wide range of the torsional angle with increasing the torsional mode quantum number. As the CH_3 torsional mode is orthogonal to the O−H extension coordinate, the reactive flux characterized by the specific CH_3 rotor level would experience the H atom tunneling barrier, which is dynamically shaped by the conical intersection extended along the corresponding CH_3 torsional seam coordinate. The tunneling barrier for the S_1 reactive flux at the eclipsed or staggered geometry is then determined by the energetics and nuclear configuration of the S_1/S_2 conical intersection with the eclipsed (crest) or staggered (trough) geometry developed along the CH_3 torsional seam coordinate, respectively. As the CH_3 torsional barrier height along the conical intersection seam coordinate ($V_3 \approx 400$ cm^{-1}) is much higher than that in S_1 ($V_3 \approx 83$ cm^{-1}), the O−H tunneling barrier is expected to be much higher for the eclipsed geometry compared to that for the staggered geometry. For instance, at the $3a_1$ torsional mode excitation at the S_1 internal energy of 74 cm^{-1}, its eigenfunction indicates that the corresponding reactive flux would be most probable in the staggered configuration, Figure 3. In this case, the tunneling barrier imposed by the S_1/S_2 conical intersection seam for the reactive flux at the $3a_1$ mode excitation is significantly lowered compared to that at the zero-point energy, rationalizing the experimental observation of the sharp increase of the tunneling rate at $3a_1$. As the quantum number of the CH_3 rotor level increases further above the torsional barrier in S_1, the preference of the initial reactive flux with respect to the CH_3 internal rotor geometry becomes diminished. Instead, tunneling occurs at the multiple configurations in terms of the CH_3 torsional angle where the tunneling barriers are diversified in the wide dynamical range. In this case, the behavior of the tunneling rate with the CH_3 torsional level excitation could be extremely well-explained by the simple model based on a dynamic shaping of the barrier along the seam coordinate of the conical intersection. The tunneling barrier for the eclipsed and/or staggered geometry is weight averaged according to the square of the wave function of each CH_3 torsional quantum level over the nuclear configuration of the entire $0-2\pi$ torsional angle, giving the estimation for the effective tunneling barrier for each CH_3 internal rotor level. The calculated effective torsional barrier then perfectly matches with the experiment, Figure 2, clearly identifying the dynamic role of the "seam" coordinate of the conical intersection. This demonstrates that the extension of the conical intersection into the seam coordinate is quite essential in dictating the multidimensional tunneling reactions. This is the first experimental demonstration that the conical intersection extended along the seam coordinate strongly influences the tunneling dynamics through shaping the underlying barrier along the H atom detachment coordinate.

For the *cis*-*o*-cresol, the S_1 lifetime turns out to be much longer than that of the *trans* conformer, giving $\tau \approx 1.8$ ns at the S_1 zero-point energy level when the biexponential fit is used (it gives $\tau \approx 5.0$ ns by a single exponential decay function fit) (vide supra). In the *cis* conformer, as the most stable staggered geometry in S_0 is unaltered in S_1,[42] the S_1-S_0 origin is most strongly observed, Figure 1. As the number of vibronic bands of the *cis* conformer is only a few, the general trend of the tunneling rate with the increasing internal energy is not obvious. Moreover, as the S_1 lifetime is quite long, the lifetime estimation is not quite certain in the present experimental setup, where the maximum reaction time is mostly limited to 2.88 ns. As above, one may fit the transient with either the single- or biexponential decay function, although the latter is more consistent with the experiment. For instance, the appearance rate of the H fragment matches the decay rate of the parent transient when the parent transient is fit with the biexponential decay function. Actually, the presence of the long-lived component becomes obvious in some transients of the *cis* conformer. In the same context, the H photofragment yield is much smaller in *cis* compared to *trans* (Supporting Information), implying that the S_1 state is mostly depopulated by the H atom detachment for the *trans* conformer, whereas the significant portion of the S_1 population undergoes the slow decaying process other than the H-tunneling in the *cis* conformer. Kinetically, the S_1 parent transient is supposed to reflect the total sum of the depopulation rates of the S_1 state, regardless of the relative quantum yield. And yet, if the long-lived component due to the internally hot ground state (S_0), triplet state (T_1),[32] or the partially trapped S_1 is somehow probed, the transient would show the biexponential decay (Supporting Information). Actually, our result strongly supports this, although further experimental studies such as time-resolved photoelectron spectroscopy would be desirable for resolving this interesting dynamic issue. The S_1/S_2 conical intersection with respect to the S_1 minimum is theoretically predicted to be located much higher in the *cis* conformer compared to that in *trans*. Thus, the adiabatic tunneling barrier for the H atom detachment in the *cis*-*o*-cresol is supposed to be much higher than that in the *trans*-*o*-cresol, rationalizing the experimental finding of the much longer S_1 lifetime of the former (see the Supporting Information).

Herein, the dynamic role of the seam coordinate of the multidimensional conical intersection was clearly revealed for the first time. The rate of the H atom tunneling reaction in the S_1 states of the *trans*-*o*-cresol shows the sharply varying behavior with the seemingly dynamically remote CH_3 torsional mode excitations. The sinusoidal potential energy function with eclipsed and staggered geometries as crest and trough, respectively, along the CH_3 internal rotor angle was identified as one of the $(3N - 8)$ dimensional seam coordinates of the S_1/S_2 conical intersection. The tunneling process taking place under the conical intersection extended into the CH_3 torsional seam coordinate is then found to be governed by the dynamically shaped multidimensional barriers, which are characterized on multiple nuclear configurations of the reactive flux. This is the first experimental observation demonstrating the important dynamic role of the seam coordinate of the conical intersection.

EXPERIMENTAL AND THEORETICAL DETAILS

The experimental details have been previously described.[28,39] Briefly, the independently tunable pump (278−261 nm) and probe picosecond laser pulses were generated by two separate optical parametric amplifier (OPA) units pumped by a 50:50

https://dx.doi.org/10.1021/acs.jpclett.0c03742
J. Phys. Chem. Lett. 2021, 12, 1854−1861

split output of a picosecond Ti:sapphire regenerative amplifier system (791 nm, 1 kHz) seeded by a femtosecond oscillator. The probe pulse wavelength of 281.0, 296.6, 310.0, or 323.4 nm was used to ionize the transient *o*-cresol in the S_1 state, whereas that of 243.1 nm was employed for the H fragment detection via the (2 + 1) ionization. The polarization of the pump laser pulse was parallel to the detector, whereas the polarization of the probe laser pulse was maintained at the magic angle (54.7°) with respect to that of the pump laser pulse. The pump and probe laser pulses were colinearly aligned and focused (nominal focus length (fl) = 300 mm) on the molecular beam in the vacuum chamber through a 1 mm thick UV-fused silica window. The laser intensity was attenuated with several neutral density filters to avoid pump- or probe-only background signals. The time-delay between pump and probe laser pulses was controlled by a 220 mm long linear translational stage on which the retroreflectors were placed. The sample of *o*-cresol (TCI, 99%) was heated to 50 °C before it was mixed with the Ne carrier gas. The mixture was then expanded into a vacuum chamber through a high-repetition (200 Hz) Even-Lavie valve with the backing pressure of ∼2.5 atm. The molecular beam was collimated by a 3 mm diameter skimmer before it was crossed by the picosecond laser pulses. The ions of parent or photofragments were repelled and extracted by the conventional velocity map electrodes[48] and detected by the position-sensitive detector equipped with the Chevron-type microchannel plates (MCP) coupled to the phosphor screen. The time-resolved ion images were collected by capturing the luminescence of a phosphor with a triggered complementary metal oxide semiconductor (CMOS)-type camera by the event-counting method.[49−51] The raw image was processed by a LabVIEW-based home-built software and reconstructed by using the polar onion peeling (POP) method.[52]

At each staggered or eclipsed geometry, the calculated $\pi\pi^*$ and $\pi\sigma^*$ potential energy curves along the O−H extension coordinate were analytically fit by the Morse-type function or the combination of the Morse and exponential functions, respectively. The two-dimensional potential curves along two orthogonal coordinates of the O−H elongation and CH_3 torsional angle is then constructed by the combination of the analytical function (for the O−H extension (r)) and the sinusoidal function (with respect to the CH_3 torsional angle (θ)). For the eigenfunction calculation, the Fourier grid Hamiltonian method[53] was employed for the analytically fit Morse potential ($\pi\pi^*$) with 512 grids in the range of the O−H distance of 0.82−1.25 Å. Along the CH_3 internal rotor coordinate, a hindered rotor Hamiltonian is set to be solved using the grid-based method with the periodic boundary condition[54] with the 1440 grid points over the range of $-\pi < \theta < \pi$. The parameters in the hindered rotor Hamiltonian (F, V_3, and V_6) of the *trans*-*o*-cresol were adopted from a previous report.[42] The resulting two-dimensional eigenfunction matrix was normalized to unity. The effective tunneling barrier heights for the kth rotor level could be estimated from the energy differences between the eigenvalues of the corresponding S_1 rotor states ($V_k^0(r,\theta)$) and the S_1/S_2 conical intersection energetic values ($V_k(r,\theta)$). They are weight-averaged according to the nuclear layouts of the reactive flux represented by the square of the corresponding two-dimensional wave function ($|\psi_k(r,\theta)|^2$). The integration over the entire r and θ then gives the effective tunneling barrier height for the kth rotor level (see Table S1 in the Supporting Information).

$$\int_{-\pi}^{\pi}\int_{0}^{\infty}[V_k(r,\theta) - V_k^0(r,\theta)]\psi_k{}^2(r,\theta)\,\mathrm{d}r\,\mathrm{d}\theta$$

It is notable that the V_k^0 represents the zero-point energy of the kth rotor level with respect to the O−H extension coordinate, and it is calculated to be 1900 cm^{-1} from the Fourier grid Hamiltonian method. This is, interestingly, approximately half of the empirical O−H vibrational frequency of S_1 phenol, 3581 cm^{-1}.[55] Further consideration of the a/e symmetry-related degeneracy gives the final estimation of the effective tunneling barrier height for each rotor state.

■ ASSOCIATED CONTENT

Supporting Information

The Supporting Information is available free of charge at https://pubs.acs.org/doi/10.1021/acs.jpclett.0c03742.

Effective tunneling barrier heights, picosecond lifetime measurement of *o*-cresol (full data), time-resolved ionization yield of *o*-cresol, time-resolved translational energy distribution of products from the velocity-map ion imaging data, ab initio potential energy curves of S_1 and S_2 states, the S_1/S_2 potential energy curves as a function of the COH bending angle (PDF)

■ AUTHOR INFORMATION

Corresponding Author

Sang Kyu Kim − *Department of Chemistry, KAIST, Daejeon 34141, Republic of Korea;* orcid.org/0000-0003-4803-1327; Email: sangkyukim@kaist.ac.kr

Authors

Kyung Chul Woo − *Department of Chemistry, KAIST, Daejeon 34141, Republic of Korea;* orcid.org/0000-0002-9387-9397

Junggil Kim − *Department of Chemistry, KAIST, Daejeon 34141, Republic of Korea*

Complete contact information is available at: https://pubs.acs.org/10.1021/acs.jpclett.0c03742

Notes

The authors declare no competing financial interest.

■ ACKNOWLEDGMENTS

This work has been supported by National Research Foundation of Korea (NRF) under Project Nos. 2018R1A2B3004534 and 2019K1A3A1A14064258.

■ REFERENCES

(1) Park, S. T.; Kim, S. K.; Kim, M. S. Observation of conformation-specific pathways in the photodissociation of 1-iodopropane ions. *Nature* **2002**, *415*, 306−308.

(2) Kim, M. H.; Shen, L.; Tao, H.; Martinez, T. J.; Suits, A. G. Conformationally Controlled Chemistry: Excited-State Dynamics Dictate Ground-State Reaction. *Science* **2007**, *315*, 1561−1565.

(3) Tao, H.; Shen, L.; Kim, M. H.; Suits, A. G.; Martinez, T. J. Conformationally selective photodissociation dynamics of propanal cation. *J. Chem. Phys.* **2011**, *134*, 054313.

(4) Filsinger, F.; Küpper, J.; Meijer, G.; Hansen, J. L.; Maurer, J.; Nielsen, J. H.; Holmegaard, L.; Stapelfeldt, H. Pure Samples of Individual Conformers: The Separation of Stereoisomers of Complex Molecules Using Electric Fields. *Angew. Chem., Int. Ed.* **2009**, *48*, 6900−6902.

(5) Chang, Y.-P.; Długołęcki, K.; Küpper, J.; Rösch, D.; Wild, D.; Willitsch, S. Specific Chemical Reactivities of Spatially Separated 3-

Aminophenol Conformers with Cold Ca^+ Ions. *Science* **2013**, *342*, 98−101.
(6) Rösch, D.; Willitsch, S.; Chang, Y.-P.; Küpper, J. Chemical reactions of conformationally selected 3-aminophenol molecules in a beam with Coulomb-crystallized Ca^+ ions. *J. Chem. Phys.* **2014**, *140*, 124202.
(7) Malis, M.; Loquais, Y.; Gloaguen, E.; Biswal, H. S.; Piuzzi, F.; Tardivel, B.; Brenner, V.; Broquier, M.; Jouvet, C.; Mons, M.; et al. Unraveling the mechanisms of nonradiative deactivation in model peptides following photoexcitation of a phenylalanine residue. *J. Am. Chem. Soc.* **2012**, *134*, 20340−51.
(8) Lobsiger, S.; Blaser, S.; Sinha, R. K.; Frey, H. M.; Leutwyler, S. Switching on the fluorescence of 2-aminopurine by site-selective microhydration. *Nat. Chem.* **2014**, *6*, 989−93.
(9) Sobolewski, A. L.; Domcke, W.; Dedonder-Lardeux, C.; Jouvet, C. Excited-state hydrogen detachment and hydrogen transfer driven by repulsive $^1\pi\sigma^*$ states: A new paradigm for nonradiative decay in aromatic biomolecules. *Phys. Chem. Chem. Phys.* **2002**, *4*, 1093−1100.
(10) Tseng, C. M.; Lee, Y. T.; Ni, C. K. H atom elimination from the $\pi\sigma^*$ state in the photodissociation of phenol. *J. Chem. Phys.* **2004**, *121*, 2459−61.
(11) Lan, Z.; Domcke, W.; Vallet, V.; Sobolewski, A. L.; Mahapatra, S. Time-dependent quantum wave-packet description of the $^1\pi\sigma^*$ photochemistry of phenol. *J. Chem. Phys.* **2005**, *122*, 224315.
(12) Ashfold, M. N. R.; Cronin, B.; Devine, A. L.; Dixon, R. N.; Nix, M. G. D. The Role of $\pi\sigma^*$ Excited States in the Photodissociation of Heteroaromatic Molecules. *Science* **2006**, *312*, 1637−1640.
(13) Vieuxmaire, O. P.; Lan, Z.; Sobolewski, A. L.; Domcke, W. *Ab initio* characterization of the conical intersections involved in the photochemistry of phenol. *J. Chem. Phys.* **2008**, *129*, 224307.
(14) Nix, M. G. D.; Devine, A. L.; Dixon, R. N.; Ashfold, M. N. R. Observation of geometric phase effect induced photodissociation dynamics in phenol. *Chem. Phys. Lett.* **2008**, *463*, 305−308.
(15) Roberts, G. M.; Chatterley, A. S.; Young, J. D.; Stavros, V. G. Direct Observation of Hydrogen Tunneling Dynamics in Photoexcited Phenol. *J. Phys. Chem. Lett.* **2012**, *3*, 348−352.
(16) Ramesh, S. G.; Domcke, W. A multi-sheeted three-dimensional potential-energy surface for the H-atom photodissociation of phenol. *Faraday Discuss.* **2013**, *163*, 73−94.
(17) Xu, X.; Zheng, J.; Yang, K. R.; Truhlar, D. G. Photodissociation dynamics of phenol: multistate trajectory simulations including tunneling. *J. Am. Chem. Soc.* **2014**, *136*, 16378−86.
(18) Yang, K. R.; Xu, X. F.; Zheng, J. J.; Truhlar, D. G. Full-dimensional potentials and state couplings and multidimensional tunneling calculations for the photodissociation of phenol. *Chem. Sci.* **2014**, *5*, 4661−4680.
(19) Zhu, X.; Yarkony, D. R. Fitting coupled potential energy surfaces for large systems: Method and construction of a 3-state representation for phenol photodissociation in the full 33 internal degrees of freedom using multireference configuration interaction determined data. *J. Chem. Phys.* **2014**, *140*, 024112.
(20) Xie, C.; Ma, J.; Zhu, X.; Yarkony, D. R.; Xie, D.; Guo, H. Nonadiabatic Tunneling in Photodissociation of Phenol. *J. Am. Chem. Soc.* **2016**, *138*, 7828−7831.
(21) Xie, W.; Domcke, W. Accuracy of trajectory surface-hopping methods: Test for a two-dimensional model of the photodissociation of phenol. *J. Chem. Phys.* **2017**, *147*, 184114.
(22) Lee, C.; Lin, Y.-C.; Lee, S.-H.; Lee, Y.-Y.; Tseng, C.-M.; Lee, Y.-T.; Ni, C.-K. Advantage of spatial map ion imaging in the study of large molecule photodissociation. *J. Chem. Phys.* **2017**, *147*, 013904.
(23) Xie, C.; Guo, H. Photodissociation of phenol via nonadiabatic tunneling: Comparison of two ab initio based potential energy surfaces. *Chem. Phys. Lett.* **2017**, *683*, 222−227.
(24) Lai, H. Y.; Jhang, W. R.; Tseng, C.-M. Communication: Mode-dependent excited-state lifetime of phenol under the S_1/S_2 conical intersection. *J. Chem. Phys.* **2018**, *149*, 031104.
(25) Lim, J. S.; Kim, S. K. Experimental probing of conical intersection dynamics in the photodissociation of thioanisole. *Nat. Chem.* **2010**, *2*, 627−632.
(26) You, H. S.; Han, S.; Lim, J. S.; Kim, S. K. ($\pi\pi^*/\pi\sigma^*$) conical intersection seam experimentally observed in the S-D bond dissociation reaction of thiophenol-d_1. *J. Phys. Chem. Lett.* **2015**, *6*, 3202−3208.
(27) You, H. S.; Han, S.; Yoon, J.-H.; Lim, J. S.; Lee, J.; Kim, S.-Y.; Ahn, D.-S.; Lim, J. S.; Kim, S. K. Structure and dynamic role of conical intersections in the $\pi\sigma^*$-mediated photodissociation reactions. *Int. Rev. Phys. Chem.* **2015**, *34*, 429−459.
(28) Woo, K. C.; Kang, D. H.; Kim, S. K. Real-time observation of nonadiabatic bifurcation dynamics at a conical intersection. *J. Am. Chem. Soc.* **2017**, *139*, 17152−17158.
(29) Woo, K. C.; Kim, S. K. Mode-specific excited-state dynamics of *N*-methylpyrrole. *Phys. Chem. Chem. Phys.* **2019**, *21*, 14387−14393.
(30) Ratzer, C.; Küpper, J.; Spangenberg, D.; Schmitt, M. The structure of phenol in the S_1-state determined by high resolution UV-spectroscopy. *Chem. Phys.* **2002**, *283*, 153−169.
(31) Pino, G. A.; Oldani, A. N.; Marceca, E.; Fujii, M.; Ishiuchi, S.-I.; Miyazaki, M.; Broquier, M.; Dedonder, C.; Jouvet, C. Excited state hydrogen transfer dynamics in substituted phenols and their complexes with ammonia: $\pi\pi^*$-$\pi\sigma^*$ energy gap propensity and *ortho*-substitution effect. *J. Chem. Phys.* **2010**, *133*, 124313.
(32) Lipert, R. J.; Bermudez, G.; Colson, S. D. Pathways of S_1 decay in phenol, indoles, and water complexes of phenol and indole in a free jet expansion. *J. Phys. Chem.* **1988**, *92*, 3801−3805.
(33) Lipert, R. J.; Colson, S. D. Deuterium isotope effects on S_1 radiationless decay in phenol and on intermolecular vibrations in the phenol-water complex. *J. Phys. Chem.* **1989**, *93*, 135−139.
(34) Nix, M. G. D.; Devine, A. L.; Cronin, B.; Dixon, R. N.; Ashfold, M. N. R. High resolution photofragment translational spectroscopy studies of the near ultraviolet photolysis of phenol. *J. Chem. Phys.* **2006**, *125*, 133318.
(35) Dixon, R. N.; Oliver, T. A. A.; Ashfold, M. N. R. Tunnelling under a conical intersection: Application to the product vibrational state distributions in the UV photodissociation of phenols. *J. Chem. Phys.* **2011**, *134*, 194303.
(36) Berden, G.; Meerts, W. L.; Schmitt, M.; Kleinermanns, K. High resolution UV spectroscopy of phenol and the hydrogen bonded phenol-water cluster. *J. Chem. Phys.* **1996**, *104*, 972−982.
(37) Grégoire, G.; Dedonder-Lardeux, C.; Jouvet, C.; Martrenchard, S.; Solgadi, D. Has the Excited State Proton Transfer Ever Been Observed in Phenol-$(NH_3)_n$ Molecular Clusters? *J. Phys. Chem. A* **2001**, *105*, 5971−5976.
(38) Sur, A.; Johnson, P. M. Radiationless transitions in gas phase phenol and the effects of hydrogen bonding. *J. Chem. Phys.* **1986**, *84*, 1206−1209.
(39) Woo, K. C.; Kim, S. K. Multidimensional H Atom Tunneling Dynamics of Phenol: Interplay between Vibrations and Tunneling. *J. Phys. Chem. A* **2019**, *123*, 1529−1537.
(40) Tembreull, R.; Lubman, D. M. Use of resonant two-photon ionization with supersonic beam mass spectrometry in the discrimination of cresol isomers. *Anal. Chem.* **1984**, *56*, 1962−1967.
(41) Appel, I.; Kleinermanns, K. Fluorescence excitation spectra of hydrogen-bonded cresol-isomers in supersonic free jets. *Ber. Bunsenges. Phys. Chem.* **1987**, *91*, 140−152.
(42) Aota, T.; Ebata, T.; Ito, M. Rotational isomers and internal rotation of the methyl group in S_0, S_1 and ion of *o*-cresol. *J. Phys. Chem.* **1989**, *93*, 3519−3522.
(43) Ito, M.; Yamamoto, S.; Aota, T.; Ebata, T. Rotational isomerism, molecular motion and hydrogen bonding as studies by supersonic jet spectroscopy. *J. Mol. Struct.* **1990**, *237*, 105−122.
(44) Suzuki, K.; Emura, Y.; Ishiuchi, S.; Fujii, M. Internal methyl group rotation in *o*-cresol studied by pulsed field ionization-ZEKE photoelectron spectroscopy. *J. Electron Spectrosc. Relat. Phenom.* **2000**, *108*, 13−20.
(45) King, G. A.; Devine, A. L.; Nix, M. G. D.; Kelly, D. E.; Ashfold, M. N. R. Near-UV photolysis of substituted phenols Part II. 4-, 3- and 2-methylphenol. *Phys. Chem. Chem. Phys.* **2008**, *10*, 6417−6429.

https://dx.doi.org/10.1021/acs.jpclett.0c03742
J. Phys. Chem. Lett. 2021, 12, 1854−1861

(46) Woo, K. C.; Kim, S. K. Real-Time Tunneling Dynamics through Adiabatic Potential Energy Surfaces Shaped by a Conical Intersection. *J. Phys. Chem. Lett.* **2020**, *11*, 6730−6736.
(47) Myszkiewicz, G.; Meerts, W. L.; Ratzer, C.; Schmitt, M. Rotational isomers of hydroxy deuterated *o*- and *m*-cresols studied by ultraviolet high resolution experiments. *Phys. Chem. Chem. Phys.* **2005**, *7*, 2142−2150.
(48) Eppink, A. T. J. B.; Parker, D. H. Velocity map imaging of ions and electrons using electrostatic lenses: Application in photoelectron and photofragment ion imaging of molecular oxygen. *Rev. Sci. Instrum.* **1997**, *68*, 3477−3484.
(49) Horio, T.; Suzuki, T. Multihit two-dimensional charged-particle imaging system with real-time imaging processing at 1000 frames/s. *Rev. Sci. Instrum.* **2009**, *80*, 013706.
(50) Lee, S. K.; Cudry, F.; Lin, Y. F.; Lingenfelter, S.; Winney, A. H.; Fan, L.; Li, W. Coincidence ion imaging with a fast frame camera. *Rev. Sci. Instrum.* **2014**, *85*, 123303.
(51) Li, W.; Chambreau, S. D.; Lahankar, S. A.; Suits, A. G. Megapixel ion imaging with standard video. *Rev. Sci. Instrum.* **2005**, *76*, 063106.
(52) Roberts, G. M.; Nixon, J. L.; Lecointre, J.; Wrede, E.; Verlet, J. R. Toward real-time charged-particle imaging reconstruction using polar onion-peeling. *Rev. Sci. Instrum.* **2009**, *80*, 053104.
(53) Marston, C. C.; Balint-Kurti, G. G. The Fourier grid Hamiltonian method for bound state eigenvalues and eigenfunctions. *J. Chem. Phys.* **1989**, *91*, 3571.
(54) Ercolani, G. Numerical evaluation of energy levels and wave functions for hindered internal rotation. *J. Chem. Educ.* **2000**, *77*, 1495.
(55) Bist, H. D.; Brand, J. C. D.; Williams, D. R. The 2750-Å band system of phenol: Part II. Extended vibrational assignments and band contour analysis. *J. Mol. Spectrosc.* **1967**, *24*, 413−467.

https://dx.doi.org/10.1021/acs.jpclett.0c03742
J. Phys. Chem. Lett. 2021, 12, 1854−1861